Molecular dynamics studies of interactions between Arg_9(nona-arginine) and a DOPC/DOPG(4:1) membrane

Cite as: AIP Advances **10**, 105103 (2020); https://doi.org/10.1063/5.0015665
Submitted: 29 May 2020 . Accepted: 09 September 2020 . Published Online: 01 October 2020

Seungho Choe

Molecular dynamics studies of interactions between Arg_9(nona-arginine) and a DOPC/DOPG(4:1) membrane

Cite as: AIP Advances 10, 105103 (2020); doi: 10.1063/5.0015665
Submitted: 29 May 2020 • Accepted: 9 September 2020 •
Published Online: 1 October 2020

Seungho Choe[a]

AFFILIATIONS

School of Undergraduate Studies, College of Transdisciplinary Studies, Daegu Gyeongbuk Institute of Science and Technology, 333 Techno Jungang-daero, Hyeonpung-eup, Dalseong-gun, Daegu 42988, South Korea

[a]Author to whom correspondence should be addressed: schoe@dgist.ac.kr

ABSTRACT

It has been known that the uptake mechanisms of cell-penetrating peptides (CPPs) depend on the experimental conditions such as the concentration of peptides, lipid composition, and temperature. In this study, we investigate the temperature dependence of the penetration of Arg_9s into a DOPC/DOPG(4:1) membrane using molecular dynamics (MD) simulations at two different temperatures, T = 310 K and T = 288 K. Although it is difficult to identify the temperature dependence because of having only one single simulation at each temperature and no evidence of translocation of Arg_9s across the membrane at both temperatures, our simulations suggest that following are strongly correlated with the penetration of Arg_9s: a number of water molecules coordinated by Arg_9s and the electrostatic energy between Arg_9s and the lipid molecules. We also present how Arg_9s change a bending rigidity of the membrane and how a collective behavior between Arg_9s enhances the penetration and the membrane bending. Our analyses can be applicable to any CPPs to investigate their interactions with various membranes using MD simulations.

I. INTRODUCTION

Cell penetrating peptides (CPPs), typically comprising 5–30 amino acids, can translocate across cell membranes. They have been extensively studied for a couple of decades since they are capable of transporting various cargoes (e.g., proteins, peptides, DNAs, and drugs) into cells.[1] However, the uptake mechanisms of CPPs are still controversial. It is known that the translocation mechanisms of different families of CPPs are not the same, and most CPPs can have more than a single pathway depending on the experimental conditions.[2] There are two major uptake mechanisms, i.e., the endocytotic (energy-dependent) pathway and the direct (energy-independent) translocation. The detailed uptake mechanisms can be found in Refs. 1–3.

The uptake mechanisms of CPPs depend on various factors such as the physical and chemical properties of CPPs, the concentration of CPPs, and the properties of the membrane.[3] The concentration of CPPs is one of the key factors that gives different uptake pathways. It is generally accepted in many CPPs that endocytosis occurs at low concentration, while the direct translocation occurs at low concentration. However, penetratin shows the reverse. Endocytosis occurs at high concentration, while the direct translocation occurs at low concentration in the case of penetratin.[4] Therefore, the uptake mechanism seems much more complicated than we thought. There are various models to explain the direct translocation, such as the carpet-like model,[5] pore formation,[6] inverted micelle formation,[7] and the membrane thinning model[8]. Detailed mechanisms of those models are also given in Refs. 2 and 3.

Among various CPPs, arginine-rich peptides seem very interesting. As mentioned above, the switch between different uptake mechanisms might depend on the concentration of the peptides. It has been shown in experiments that endocytosis is only dominant to a specific low peptide concentration.[9] One of the possible scenarios for the insertion of arginine-rich peptides into the lipid bilayer

is a strong interaction with negatively charged phospholipid heads (see, e.g., Ref. 3). The charge neutralization results in the membrane deformations, and this can lead to a decrease in the bending rigidity of the membrane.

The rapid cytoplasmic entry has been explained by the accumulation of the peptides at certain membrane areas, called nucleation zones.[10] It was also reported that a rapid temperature decrease from 37 °C to 15 °C induces an efficient entry of Arg_9 (called R9 or nona-arginine in different literature) even at a low peptide concentration.[11] This is why two temperatures (T = 310 K and 288 K) were chosen in our simulations. Although the mechanism of temperature dependence shown in Ref. 11 is closely related to calcium signaling, we focus primarily on the temperature dependence of interactions between Arg_9 and the lipid molecules.

It was shown by Eiríksdóttir *et al.*[12] that several CPPs can adopt a specific secondary structure in stabilizing their interactions with membranes. Among them, Arg_9 exhibited a random coil in both water and membrane environments, and it means that Arg_9 was unable to adopt any specific secondary structure in both environments. Eiríksdóttir *et al.*[12] also carried out leakage tests to assess the consequence of interactions between Arg_9 and membranes on membrane stability and found that Arg_9 did not induce any leakage, suggesting no membrane perturbation and probably no insertion into the bilayer.

It was suggested that the entry of Arg_9 into DOPG/DOPC-GUV(GUV: the giant unilamella vesicle) and DLPG/DTPC(2/8)-GUV occurs through transient hydrophilic prepores.[13] A prepore is an area of decreased density of lipids due to the fluctuations of local lateral density. Prepores immediately close because of the large line tension. The interaction of CPPs with these prepores may stabilize the prepores by decreasing their line tension. More detailed physical views on prepores and comparison of the line tension of several lipid mixtures are given in Ref. 13 and references therein.

Herce *et al.*[14] showed in their molecular dynamics (MD) simulations that Arg_9 follows the same mechanism previously found for Tat[15] by the same authors. The attractive interactions between the Arg_9 peptides and the phosphate groups of the phospholipids result in large local distortions of the bilayer, and these distortions lead to the formation of a toroidal pore. Note that the authors used the system containing a single phospholipid (DOPC) in their MD simulations. However, the authors showed in experiments that anionic phospholipids such as DOPG lipids are not required for the Arg_9 peptides to penetrate bilayers.[14]

MD simulations have been used to investigate functional properties of Arg_9 and its interactions with many different lipids; however, only a few simulations used mixtures of lipids (e.g., a mixture of DOPC/DOPG or DOPC/DOPE) so far, and the mechanism of translocation of Arg_9 and interactions with lipids are still not conclusive. It was found that a DOPC/DOPG membrane appeared to be the better host for the translocation of KR9C in MD simulations.[16]

In our study, we investigate the penetration of Arg_9 peptides into a model membrane [e.g., a mixture of DOPC/DOPG(4:1)] using MD simulations at two different temperatures (T = 310 K and T = 288 K). Our first goal is to see if Arg_9 can translocate across the DOPC/DOPG mixture by making a pore or a prepore, and the second goal is to investigate the temperature dependence of interactions between Arg_9 and the lipid mixture.

II. SIMULATION METHODS

All simulations were performed using the NAMD package[17] and CHARMM36 force field.[18] CHARMM-GUI[19] was used to set up a DOPC/DOPG(4:1) mixture and TIP3P water molecules. The lipid mixture consists of 76 DOPC and 19 DOPG lipids in each layer. K and Cl ions were added to make a concentration of 150 mM. One Arg_9 peptide was made by the molefacture plugin in visual molecular dynamics (VMD),[20] and it was duplicated to make four Arg_9 peptides. The total number of Arg_9 peptides was the same as in Herce *et al.*'s[14] to make a similar concentration of Arg_9s. All Arg_9 peptides were initially located in the upper solution, and they were bound to the upper layer during the equilibration. The total number of water molecules after making the system neutralized was 9643. The NPT simulations were performed at two different temperatures T = 288 K and 310 K in order to investigate the temperature dependence of penetration of Arg_9s. The temperature and pressure were kept constant using Langevin dynamics. An external electric field (0.05 V/nm) was applied in the negative z direction (from the Arg_9 peptides to the membrane) as suggested in the previous work[14,21] to account for the transmembrane potential.[22] The particle-mesh Ewald (PME) algorithm was used to compute the electric forces, and the SHAKE algorithm was used to allow a 2 fs time step during the whole simulations. At the first stage, the system was equilibrated at T = 310 K for 500 ns long. At the second stage, two systems were prepared: One was a system with the same temperature (T = 310 K) as in the equilibration at the first stage. The other was a system with T = 288 K. When the temperature was down from T = 310 K to T = 288 K in the second system, the system was quickly equilibrated at T = 288 K. Both systems (T = 310 K and 288 K) were ran for another 500 ns. The first 200 ns data in both simulations were discarded for the equilibration, and only the last 300 ns data were used for the analyses.

III. SIMULATION RESULTS

A. A number of water molecules coordinated by Arg_9s are strongly correlated with the penetration depth

We do not see any translocation of Arg_9 across the DOPC/DOPG bilayer during the simulations. However, it can penetrate into the lipid mixture along with a quite number of water molecules. We define the penetration depth as the distance in the z direction between the center of mass of each Arg_9 (taking only C_αs for the sake of simplicity) and that of the upper leaflet. Here, a leaflet means a surface that consists of 95 phosphorus (P) atoms in the upper or the lower layer.

Figure 1(a) shows the penetration depth of each Arg_9 at T = 310 K. The solid lines denote the penetration depth of each Arg_9, and the dotted line represents an average over those four values. The positive value means that the center of mass of Arg_9 is located above the center of masses of phosphorus (P) atoms, and the negative value means below the phosphorus (P) atoms. One of Arg_9s(Arg3) is located below the upper leaflet during most the of simulation time.

Figure 1(b) shows the same quantity as in Fig. 1(a), but at T = 288 K. It shows that Arg_9 can penetrate slightly more into the lipid mixture at T = 288 K. One of Arg_9s(Arg3) is below the upper leaflet during the whole simulation time, and it reaches even −5 Å

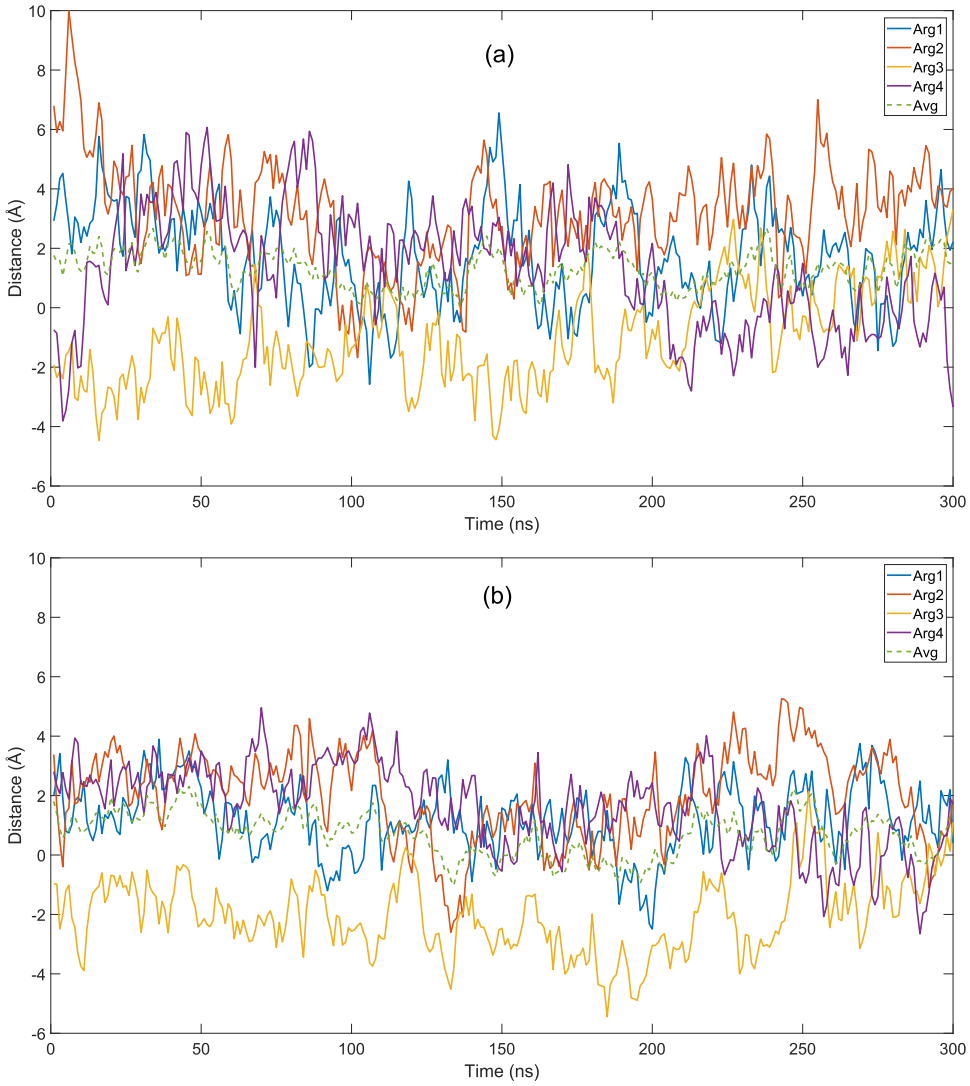

FIG. 1. Distance between the center of mass of each Arg_9 and the center of masses of phosphorus (P) atoms in the upper leaflet (in the z direction) at (a) T = 310 K and (b) T = 288 K, respectively. The color code represents each Arg_9. Avg (green dotted line) means an average value over four Arg_9s.

in this figure. Note that each point in the figures corresponds to a block average over 1 ns. We find that the largest penetration depth is −6.3 Å during the simulation at T = 288 K, and Fig. 2 shows a snapshot at that moment. C_αs of Arg3 are shown in the same color code in Fig. 1. The green dots by the vdW representation of VMD correspond to phosphorus (P) atoms in the DOPC/DOPG mixture. The lipid molecules are shown as gray lines, and water molecules are represented by vdW of VMD. Figure 3 presents a deformation of the upper leaflet due to the presence of Arg_9s and a relative distance between the upper leaflet and each Arg_9 using the snapshot in Fig. 2. The lower leaflet is not shown in this figure for clarity. The blue color in the leaflet denotes a trough and the yellow a crest. Some of C_αs located below the leaflet are not seen in this figure.

A quite number of water molecules also penetrate into the DOPC/DOPG mixture, and this results in membrane thinning and bending. Figure 4 shows the total number of water molecules located 15 Å apart from the center of mass of Arg3 at T = 288 K. We count only water molecules below the center of masses of phosphorus (P) atoms. Figure 4 shows a strong correlation between the penetration depth of Arg_9 and the number of water molecules surrounding it. The number of water molecules increases as the penetration of Arg3 increases. This confirms the previous results from MD simulations.[23–25]

At the current stage, we cannot conclude that the lowering temperature will really help Arg_9s to make more penetration into the lipid mixture. First of all, the difference in average penetration depths at two temperatures is not that significant (about 1 Å or 2 Å on average). Second, we have only one single simulation at each temperature, and the total simulation time (300 ns) may not be long enough to see the temperature dependence. However, it turns out that the penetration depths are affected by the electrostatic energy between Arg_9s and the lipid mixture, and we want to focus on how Arg_9s interact with the lipid mixture in the following analyses.

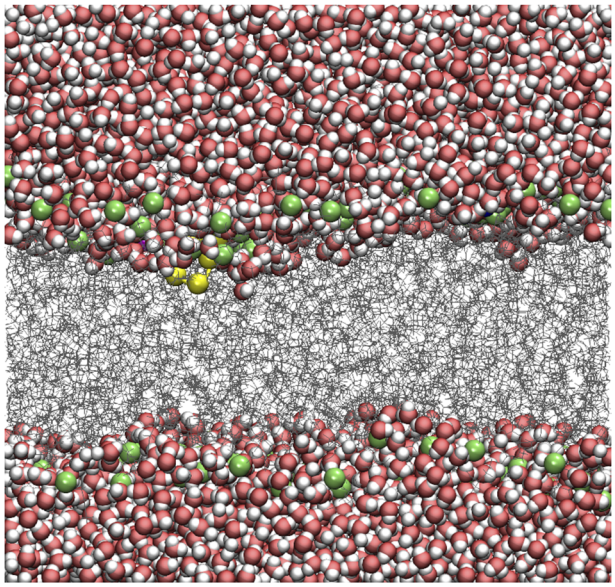

FIG. 2. A snapshot that shows the largest penetration depth of Arg3 (yellow) at T = 288 K. Only Arg3 (yellow), the phosphorus (P) atoms (green dots), the lipid molecules (gray lines), and the water molecules in vdW of VMD are shown.

B. Electrostatic energy between Arg_9s and the DOPC/DOPG mixture is important for penetration

It is difficult to imagine how Arg_9s can pass through the DOPC/DOPG mixture because DOPG is a negatively charged lipid, and therefore, one can expect strong attractive interactions between Arg_9s and DOPG lipids. It was suggested that the electrostatic interaction between positive charges of Arg_9s and negative charges of lipid molecules is crucial at the early stage of translocation.[21] We want to investigate this feature in our simulations.

We calculate the electrostatic energy between each Arg_9 and the DOPC/DOPG mixture at both temperatures using the NAMD Energy plugin in VMD. We want to see if there is any correlation between the strength of electrostatic energy and the penetration depth. Figure 5(a) shows the electrostatic energy between each Arg_9 and the DOPC/DOPG mixture at T = 310 K. Each color code (the same color scheme as in the previous figures) represents the interaction between one of Arg_9s and the lipid mixture. Avg denotes an average energy over all four Arg_9s. Figure 5(b) shows the same energy, but at T = 288 K. The average electrostatic energy at T = 288 K is slightly lower (more stable) than that at T = 310 K by 100 kcal/mol. This can be explained by comparing the average penetration depths in Figs. 1(a) and 1(b). Arg_9 can penetrate slightly more at T = 288 K because of a lower electrostatic energy. Note that in Fig. 5(b), one of the lowest energy regions (170 ns–200 ns) corresponds to a region that shows the largest penetration depth in Fig. 1(b). One can see a similar behavior in the case of Arg1 (blue) at about 200 ns in Figs. 1(b) and 5(b). In both Figs. 5(a) and 5(b), the electrostatic energy between Arg3 (yellow) and the lipid mixture increases (less stable) at the end of simulation because the penetration depth of Arg3 decreases as shown in Figs. 1(a) and 1(b), respectively. Our simulations clearly suggest that the electrostatic energy plays a key role in controlling the penetration depth of Arg_9.

Then, the next question will be whether Arg_9 can make a pore or a prepore in the presence of a strong electrostatic energy between Arg_9s and the lipid mixture. At this stage, it is not clear how this can happen, but we think that Fig. 2 can give us a clue. In Fig. 2, one can observe a quite number of water molecules coordinated by Arg3 when it makes the largest penetration through the lipid mixture at T = 288 K. It was known by molecular dynamics simulations that water molecules can enhance membrane bending and disorder the lipid molecules.[23–25] We conjecture that the concentration of Arg_9s

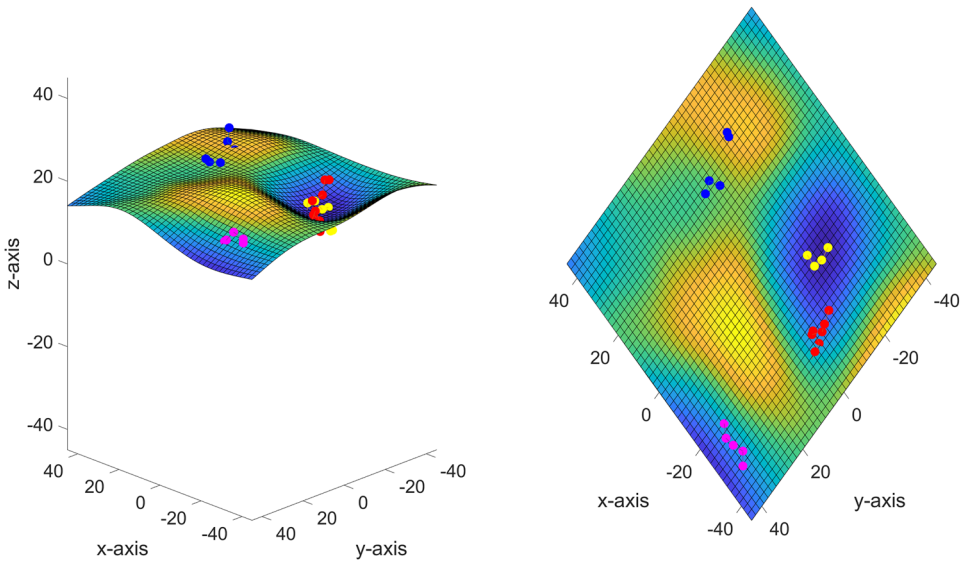

FIG. 3. Membrane curvature and a relative position of each Arg_9 (showing C_αs only) from the snapshot in Fig. 2. Representation in 3D (left) and in the x–y plane (right), respectively.

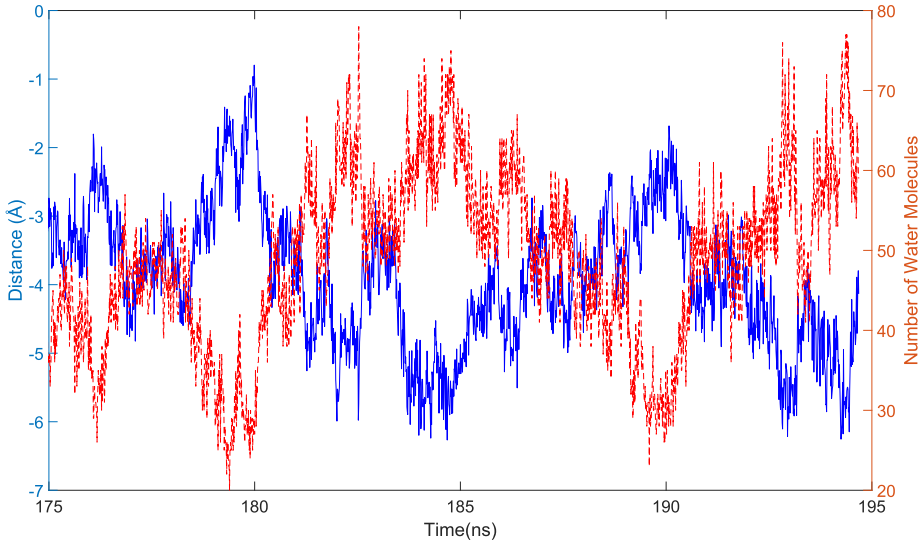

FIG. 4. Distance between the center of mass of Arg3 and the center of masses of 95 phosphorus (P) atoms in the upper leaflet (blue solid line, the left axis) and a number of water molecules within 15 Å of Arg3 (red dotted line, the right axis) at T = 288 K. We count only water molecules below the center of masses of P atoms.

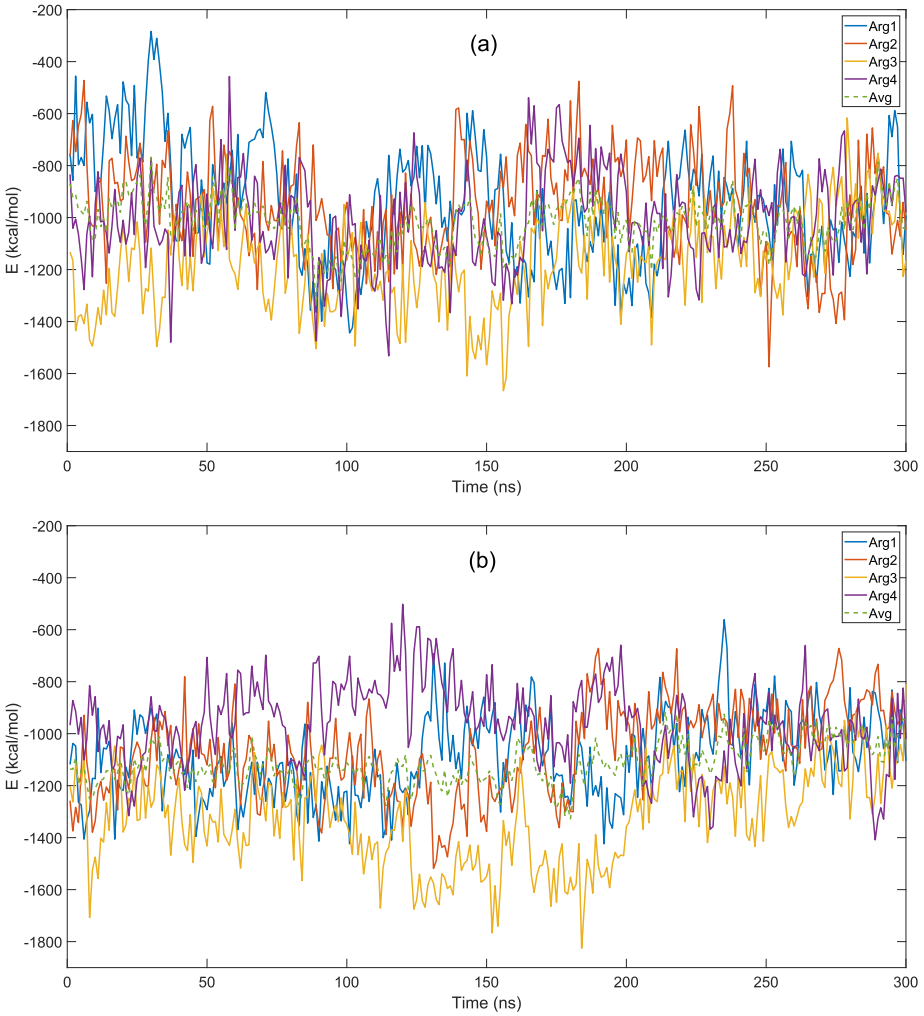

FIG. 5. Electrostatic energy between Arg_9s and the DOPC/DOPG lipids at (a) T = 310 K and (b) T = 288 K. The same color code in Fig. 1 is used. Avg (green dotted line) means an average value over four Arg_9s.

will be one of the key factors to coordinate more water molecules. More water molecules will accelerate the membrane bending and thinning, and thus, there may be more interactions between Arg_9s and the lipid molecules in the lower layer. However, the concentration of Arg_9s in our simulations seems not large enough to see this behavior. In Appendix A, we present membrane thinning due to the penetration of Arg3. It is obvious that the increase in penetration of Arg_9s results in membrane thinning. The detailed method to obtain the distance between the layers is explained in Appendix A. More details on membrane bending are given below.

C. Bending rigidity of the membrane is decreased due to the presence of Arg_9s

It was shown that there is a correlation between CPP hydropathy and the penetration of water molecules in the lipid bilayer and the presence of water molecules locally destabilizes the lipid order and reduces a bending modulus of the membrane.[26] The reduction in membrane bending rigidity has also been reported in other literature.[3,16]

We compare bending moduli of the DOPC/DOPG mixture at two different temperatures (T = 288 K and 310 K). We compute the bending moduli using the method described in Refs. 26–28. A similar approach to calculate the bending moduli of various lipid molecules was suggested by Levine *et al.*[29] The authors also tried Khelashvili *et al.*'s method[28] to analyze their data and found that their bending moduli are consistent with Khelashvili *et al.*'s. We use Khelashvili *et al.*'s method for obtaining the bending modulus of the membrane, and this will be enough to see the temperature dependence of the bending moduli in our simulations.

It was shown that one can calculate the splay modulus χ by calculating splay angles (α) between lipid molecules. We use the same definition of a splay angle in Refs. 26–28 (see more in Appendix B).

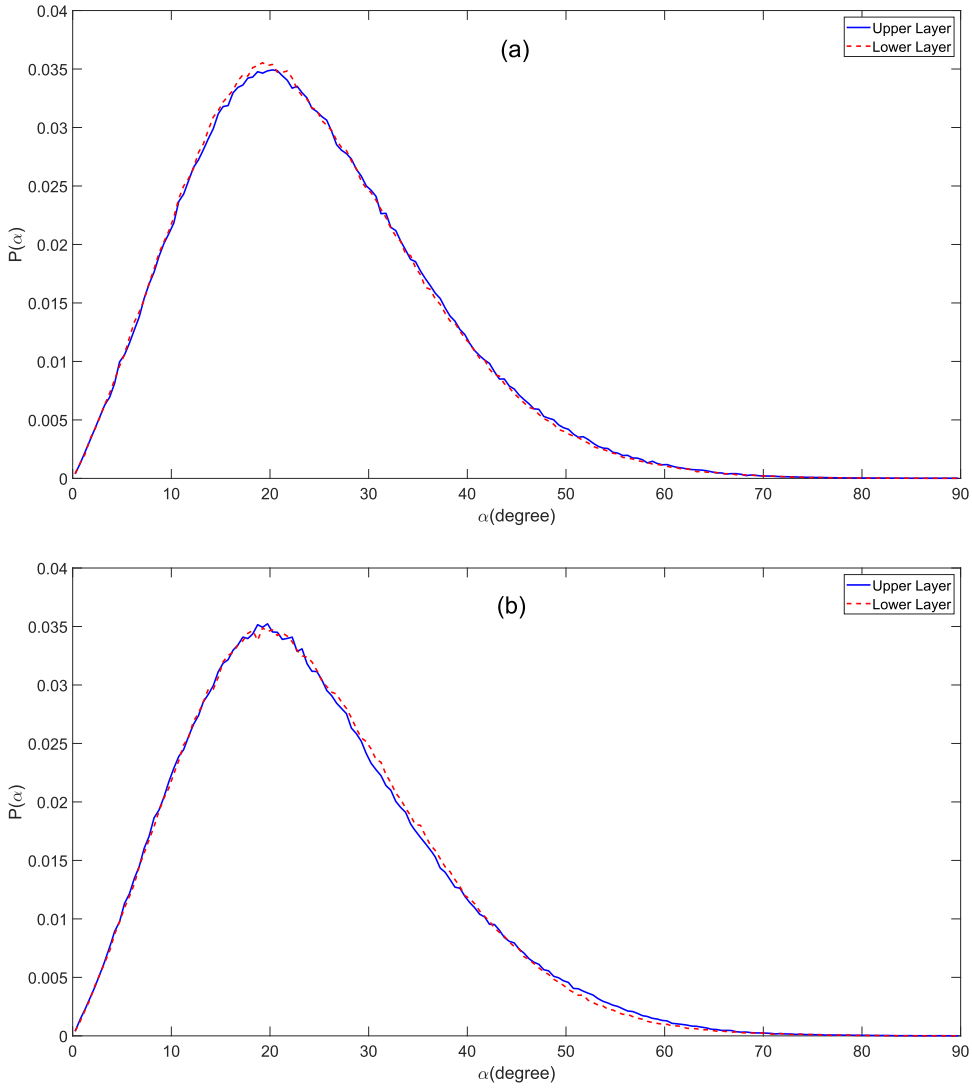

FIG. 6. Normalized probability distributions of α at (a) T = 310 K and (b) T = 288 K. The blue solid line denotes a distribution from the upper layer, while the red dotted line comes from the lower layer.

There are two criteria to analyze the splay angles as explained in the previous work:[28,29] (1) Only lipid pairs separated by less than 10 Å are considered. (2) At least one director should be oriented less than or equal to 10° from the bilayer normal. In this approach, a normalized probability distribution is used to calculate the potential of mean force (PMF). The PMF is defined by

$$\mathrm{PMF}(\alpha) = -k_B\mathrm{T}\ \ln\frac{P(\alpha)}{P_0(\alpha)}, \tag{1}$$

where $P_0(\alpha) = \sin(\alpha)$ is the probability distribution of a hypothetical non-interacting particle system, k_B is the Boltzmann factor, and T is the temperature. The splay modulus χ is obtained by a quadratic fit of the PMF data, and it corresponds to the bending modulus of a monolayer K_m. The presence of Arg_9, e.g., in the upper layer, also affects the bending modulus of the lower layer. Therefore, we compute the bending modulus K_c of a bilayer by averaging two moduli from each layer.

Figure 6(a) shows normalized probability distributions of α, $P(\alpha)$, at T = 310 K. The blue solid line is a distribution from the upper layer, while the red dotted line comes from the lower layer. Two lines are almost overlapped with each other, and the same behavior is seen in probability distributions at T = 288 K [see Fig. 6(b)]. From the second order polynomial fitting of Eq. (1) as described in Refs. 26, 28, and 29, we obtain $K_c(310\ \mathrm{K}) = 7.6 \times 10^{-20}$ J and $K_c(288\ \mathrm{K}) = 6.8 \times 10^{-20}$ J as bending moduli of the DOPC/DOPG mixture (see Figs. 11 and 12 for the quadratic fits). The bending modulus at T = 288 K is slightly smaller, but the difference is minimal. Our values (17–18 k_BT) are slightly smaller than an experimental value, 20 k_BT ± 1 k_BT.[30] This is due to the penetration of water molecules which play a role in softening the lipid mixture.

D. A collective behavior between Arg_9s enhances penetration and membrane bending

Li *et al.*[31] found that it is difficult for a single peptide to penetrate through the membrane, while multiple peptides can translocate across membranes by making a pore. Hu *et al.*[32] also showed that the

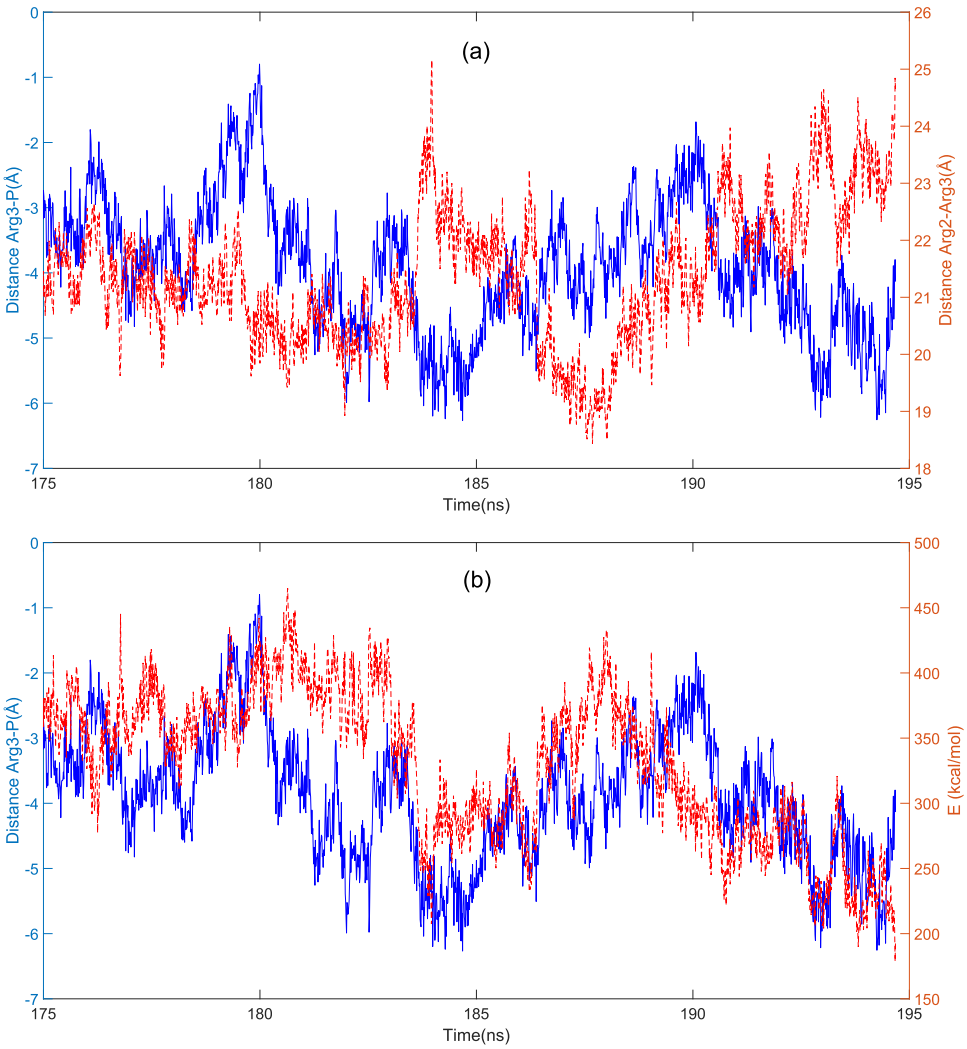

FIG. 7. Penetration depth of Arg3 (blue solid line, the left axis) at T = 288 K and (a) distance between Arg2 and Arg3 (red dotted line, the right axis) and (b) electrostatic energy between Arg2 and Arg3 (red dotted line, the right axis), respectively.

water pore formation is facilitated by the aggregated charged peptides, and the authors claimed that the cooperative effect from global and local disturbance of membranes by random and aggregated peptides results in the pore formation.

Although we do not see any translocation of Arg_9s during our simulations, our simulation results are consistent with the above findings that the collective behavior between Arg_9s significantly changes a local membrane curvature and results in more penetration into the lipid mixture. In Fig. 3, one can see that two Arg_9s (red and yellow) come closer and make a significant change in membrane bending and thinning (see also Appendix A and Fig. 10 for membrane thinning).

First, we investigate a relation between the penetration depth of Arg3 (yellow) and the distance between the center of mass of Arg2 (red) and that of Arg3 (yellow). In Fig. 7(a), the blue solid line denotes the penetration depth of Arg3 and the red dotted line shows the distance between Arg2 and Arg3. We show only data from 175 ns to 195 ns, which include the moment of the largest penetration depth of Arg3. Whenever Arg3 is trying to reach one of the largest penetration depths (e.g., about −6 Å at 184 ns or at 193 ns), the distance between Arg2 and Arg3 is going to increase rapidly.

We have another plot that shows a comparison between the penetration depth of Arg3 and the electrostatic energy between Arg2 and Arg3. We expect that the finding in Fig. 7(a) regarding the distance between Arg2 and Arg3 could be related to the electrostatic energy between Arg2 and Arg3, and this analysis will give an idea why the distance between Arg2 and Arg3 is slightly reduced when Arg3 makes the maximum penetration depth at 184.68 ns in Fig. 7(a). In Fig. 7(b), the blue solid line is the same as in Fig. 7(a) (the penetration depth) and the red dotted line is the electrostatic energy between Arg2 and Arg3. Whenever Arg3 reaches the maximum penetration, the electrostatic energy between Arg2 and Arg3 becomes the minimum (or less repulsive).

The induction of a curvature by association of proteins with the membrane has been well known for the so-called curvature sensing proteins.[33] For example, it was known that if one protein induces a given membrane curvature, it attracts more proteins that favor a similar curvature.[34] It was also shown that curvature-inducing proteins experience attractive short-range interactions due to a membrane curvature, and this curvature-mediated interaction leads to protein aggregation.[35] In order to estimate membrane-mediated interactions (attractive or repulsive potential) between Arg_9s, we need to consider long-range interactions such as entropic membrane fluctuations;[36,37] however, we want to focus primarily on a cooperative effect between Arg_9s, which affects the penetration depth and membrane bending. Our electrostatic energy calculations seem to be enough to show this feature.

We want to briefly mention the usefulness of membrane curvatures such as the mean curvature (H) or the Gaussian curvature (K) in our simulations.[38] Each curvature is defined by

$$H = \frac{1}{2}(c_1 + c_2), \qquad K = c_1 c_2, \tag{2}$$

where c_1 and c_2 are the principal curvatures at a point on the membrane. Figure 8 presents the mean curvature and the Gaussian curvature of the membrane in the presence of Arg_9s when Arg_3 shows the largest penetration at T = 288 K (see also Fig. 3). The blue color in the figure means a negative curvature, while yellow denotes a positive curvature. As we expect, the mean curvature near Arg2 (red) and Arg3 (yellow) is negative, which means a concave deformation. We have checked that the Gaussian curvature near Arg3 is always positive during the simulation at T = 288 K, which means no evidence of the pore formation.[38]

We expect that both the concentration of Arg_9s and the collective behavior are important in translocation. More simulation studies with different concentrations of Arg_9s may be necessary to gain more insights into the collective behavior.

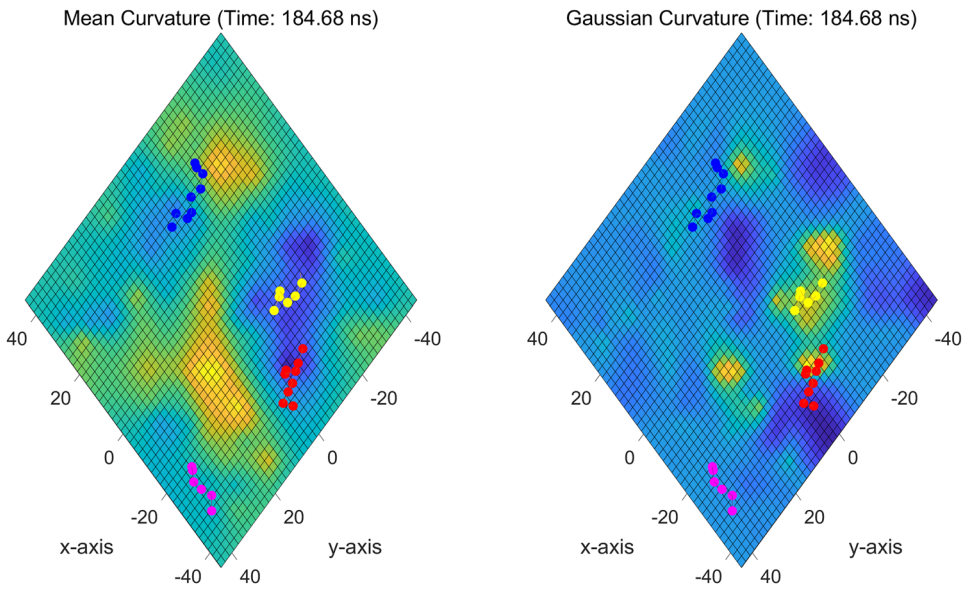

FIG. 8. Mean curvature (left) and Gaussian curvature (right) of the membrane in the presence of Arg_9s (showing only C_αs) when Arg3 (yellow) makes the largest penetration at T = 288 K. The blue color in each curvature means a negative value, while yellow denotes a positive value.

IV. DISCUSSION

Our simulations show that Arg_9 can penetrate into the DOPC/DOPG mixture, but it cannot pass through the mixture both at T = 310 K and at T = 288 K. It does not show any pore or prepore as suggested in Refs. 13 and 14. Although we do not see any translocation of Arg_9, our simulations suggest that the electrostatic energy between Arg_9 and the lipid mixture plays a role in determining the penetration depth. A few remarks regarding our results are given below.

The role of the Arg side chain was identified in the previous MD simulations.[14] The Arg side chains bind to the phosphate groups of the phospholipids; then, this binding makes large distortions of the bilayer, which lead to the formation of a pore.

Our simulation shows that more than 70 water molecules also penetrate into the lipid mixture when Arg_9 reaches the maximum penetration depth (see Fig. 4); however, Arg_9s in our simulations do not make such strong distortions in the DOPC/DOPG mixture, which can lead to a pore. We expect that the translocation may be difficult at low concentration of Arg_9s due to the attractive potential energy between Arg_9s (positive charge) and DOPG lipids (negative charge). We find that all Arg_9s were strongly bound to the DOPG lipids during the simulations. We conjecture that the ability of the translocation can be highly dependent on the concentration of Arg_9s. To our knowledge, it is not yet known how positively charged Arg_9s pass through the DOPC/DOPG mixture within all-atom MD simulations. One of the crucial reasons will be a simulation timescale. It was claimed that spontaneous translocation is not expected within timescales accessible to MD simulations, unless nonphysical restraints are applied to accelerate the underlying process.[39] In that case, a path sampling approach (e.g., the weighted ensemble method[40]) might be one of the solutions to reveal the underlying mechanism of the translocation of Arg_9s.

It was known that charged surfaces are more rigid than neutral ones; therefore, the decrease in membrane rigidity could be explained by considering that the arginine-rich peptide partially neutralizes the membranes.[16] Crosio *et al.*[16] claimed based on their experiments in the DOPC/DOPG(1:1) environment that the recruiting of the anionic DOPG lipids in the regions close to the arginine-rich peptide would lead to an enrichment of DOPC lipids in other regions, subsequently decreasing the observed bending rigidity. The incorporation of water coupled with peptide translocation and local membrane thinning can be another explanation for the reduced bending rigidity of the membrane.[26] Our simulations suggest that both the partial neutralization and membrane thinning affect softening of the DOPC/DOPG mixture. As we mentioned above, Arg_9s are strongly bound to DOPG lipids during the simulations, and this results in the partial neutralization of the membrane. We also showed membrane thinning due to the penetration of water molecules in Sec. III A. It will be interesting to investigate which factor (the neutralization or membrane thinning) can contribute more to the softening of the membrane. This can be done using different concentrations of Arg_9s as well as using different DOPC/DOPG ratios.

Although the total number of Arg_9s and the system size may not be large enough to clearly show the collective behavior in our simulations, our results suggest that it can affect the membrane bending and thinning and thus the penetration of Arg_9s. Movie S1 shows how each Arg_9 makes membrane deformations during the time frame between 175 ns and 195 ns, which includes the moment that Arg3 shows the largest penetration depth at about 185 ns. One can see in this movie that there are two main local minima made by Arg1 (blue) and Arg3 (yellow). Arg2 (red) is already closer to Arg3 (yellow), and it is trapped in a local minimum during this time frame. One interesting finding is that sometimes, two local minima are connected to each other, and this results in a drastic change in the membrane bending (see, e.g., at 188.6 ns, 190.4 ns, and 191.6 ns in the movie). One can find an increased penetration depth and a drastic decrease in the electrostatic energy of Arg1 (blue) at about 190 ns–200 ns in Figs. 1(b) and 5(b), respectively. We compute the

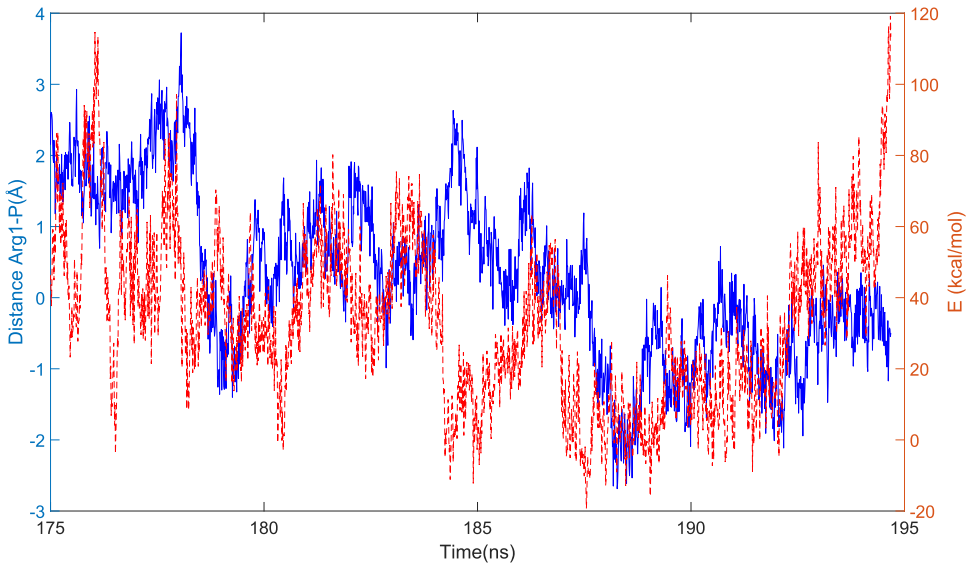

FIG. 9. Penetration depth of Arg1 (blue solid line, the left axis) at T = 288 K and the sum of the electrostatic energy between Arg1 and Arg2 and that between Arg1 and Arg3 (red dotted line, the right axis).

electrostatic energy between Arg1 (blue), Arg2 (red), and Arg3 (yellow) as we did previously for the interaction between Arg2 and Arg3. Figure 9 presents these calculations with the penetration depth of Arg1 for comparison. The blue solid line is the penetration depth of Arg1, and the red dotted line is the sum of two electrostatic energies: One is the electrostatic energy between Arg1 and Arg2, and the other one is that between Arg1 and Arg3. There is an interesting energy drop at about 185 ns, and this time frame corresponds to the moment that Arg3 makes the maximum penetration depth. One can see that the penetration increases at the time frames mentioned above, i.e., at 188.6 ns, 190.4 ns, and 191.6 ns, and the electrostatic energy becomes minimum (or less repulsive) at these time frames. It shows that there exists the collective behavior between Arg_9s, which enhances the disorder of the membrane. Further simulations with more detailed curvature analyses[33,38] will be helpful to identify the factors (e.g., the concentration of Arg_9s and the distribution of DOPG lipids in the DOPC/DOPG mixture), which control the collective behavior between Arg_9s and their effects on membrane bending.

V. CONCLUSION

The uptake mechanisms of CPPs have been extensively studied in both experiments and computer simulations. However, they are not still conclusive. The difficulty comes from the fact that the uptake pathway is not the same for different families of CPPs and depends on the experimental conditions.[2] There is no doubt that an MD simulation is still one of the valuable tools to reveal functional and mechanical properties of different families of CPPs and their interactions with various types of lipid membranes.

Our simulations suggest that the electrostatic interaction between Arg_9s and the lipid molecules is important at the early stage of the penetration, and water molecules coordinated by Arg_9s cause membrane thinning, which results in softening of the bending rigidity of the membrane. The collective behavior between Arg_9s also plays a role in helping the penetration of Arg_9s into the membrane. Although we do not see any direct translocation of Arg_9 across the DOPC/DOPG bilayer in our simulations, our analyses will be helpful for understanding functional properties of other CPPs and their interactions with various membranes using MD simulations.

SUPPLEMENTARY MATERIAL

See the supplementary material for the supplemental movie S1.

ACKNOWLEDGMENTS

The author thanks Hanna Salman and Xiao-lun Wu for valuable comments on the early stage of this work, and he also thanks the University of Pittsburgh for support during his stay. This work was supported in part by the start-up fund from the Daegu Gyeongbuk Institute of Science and Technology (DGIST).

APPENDIX A: MEMBRANE THINNING DUE TO THE PENETRATION OF Arg_9

We investigate a relation between the penetration depth of Arg3 (one of Arg_9 peptides in our simulations) and the membrane thickness at T = 288 K (see Fig. 10). When the penetration depth of Arg3 increases, the membrane thickness near Arg3 is expected to be decreased. The first panel represents the penetration depth of Arg3 [the distance between the center of mass of Arg3 and the center of masses of phosphorus (P) atoms in the upper leaflet, where a leaflet is a surface that consists of 95 phosphorus (P) atoms in each layer] between 150 ns and 300 ns. The negative value means that the center of mass of Arg3 is below the center of masses of phosphorus (P) atoms, and the positive value means the reverse. The second panel shows time variations of the membrane thickness due to the penetration of Arg3. The smallest thickness is about 27 Å, which is almost 10 Å smaller than that of a membrane without any interactions with Arg_9s (a rest state). We compute the membrane thickness as follows: First, we find the three nearest

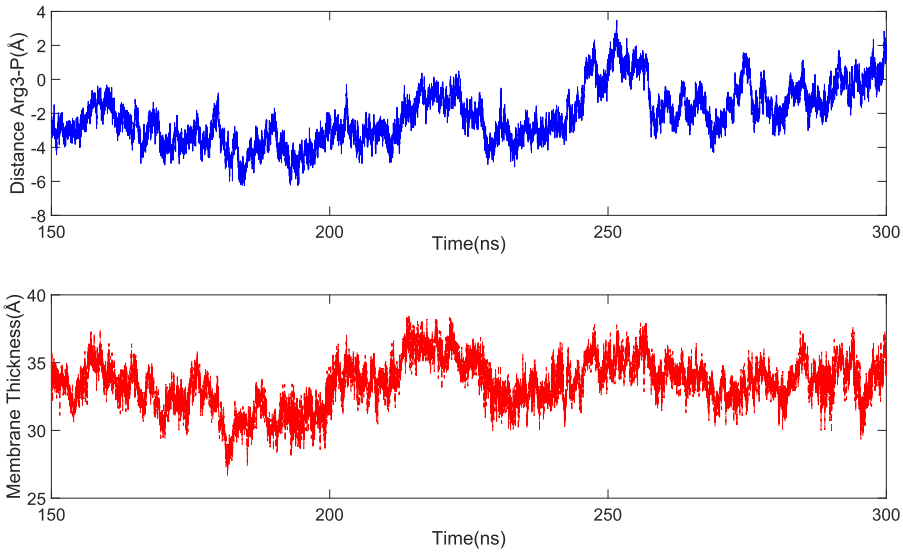

FIG. 10. Penetration depth of Arg3 (the upper panel) and membrane thickness (the lower panel) at T = 288 K.

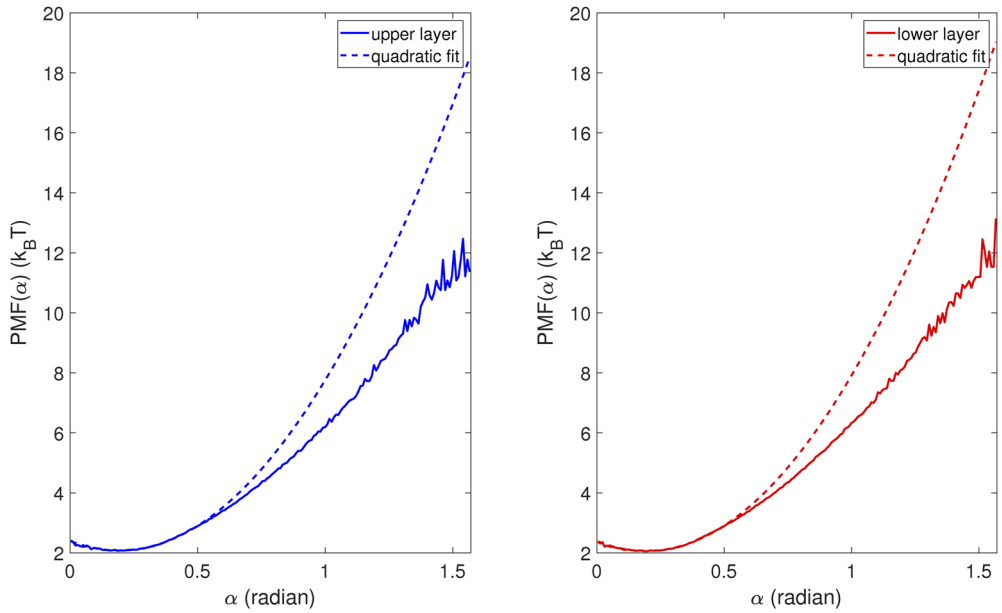

FIG. 11. PMF profiles and quadratic fits for both the upper and the lower layers at T = 310 K. The blue solid line and the blue dotted line in the left figure are a profile from the upper layer and a quadratic fit at [10°, 30°], respectively. The right figure is the same, but from the lower layer.

phosphorus (P) atoms in the upper leaflet from the center of mass of Arg3 and calculate an average z position of these three atoms. Next, we do the same thing in the lower leaflet, namely, we obtain another average z position of three nearest phosphorus (P) atoms in the lower leaflet. Then, we define membrane thickness as the distance between those two z positions. One can see that two figures show a very similar trend. This is what we exactly expected. We choose Arg3 because it shows the largest penetration depth at T

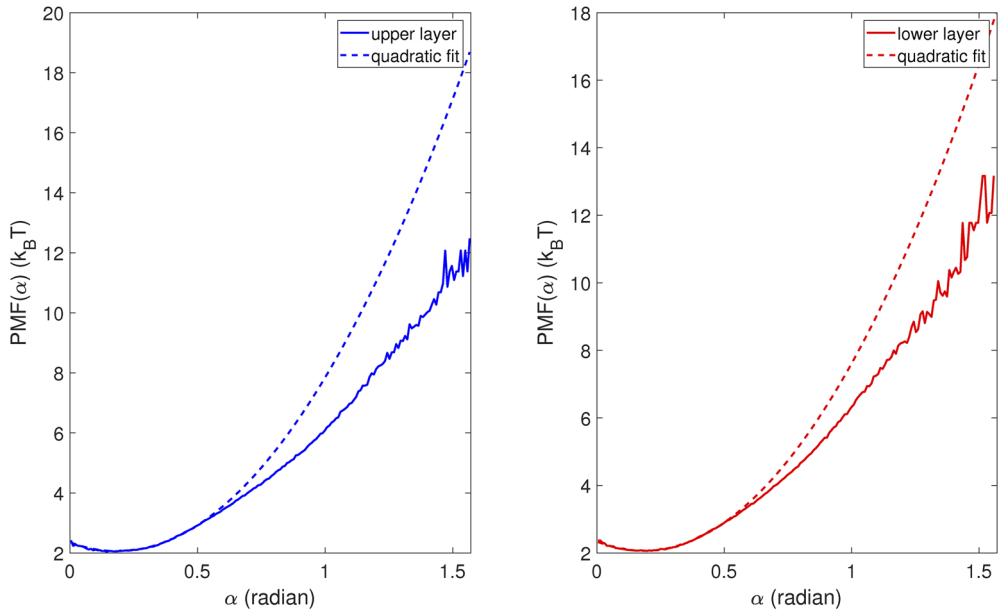

FIG. 12. The same figure as Fig. 11, but at T = 288 K.

= 288 K. The other Arg_9s can have different patterns in the membrane thickness.

APPENDIX B: BENDING MODULUS OF THE DOPC/DOPG MIXTURE

One of the mechanical properties of a membrane is its bending modulus. It was known that the penetration of a quite number of water molecules plays a role in decreasing the bending rigidity of a membrane. We investigate the bending modulus of the DOPC/DOPG mixture in the presence of Arg_9s both at T = 310 K and at T = 288 K. We use Khelashvili *et al.*'s approach[28] to get the bending modulus from MD simulations. One can compute a bending modulus from a probability distribution of splay angles. Here is a general method to obtain splay angles.[28] First, the local lipid director vector $\vec{v}$ is defined, where $\vec{v}$ is the vector that connects the midpoint between the phosphate and backbone C2 atoms to the center of mass of the three terminal carbon atoms on the two lipid chains. The splay modulus for a particular pair of lipid molecules is calculated by defining a splay angle (α) between $\vec{v}$ vectors and constructing probability distributions $P(\alpha)$ (see the main text and Ref. 28). Figure 11 presents the potential of mean force (PMF) profile $\mathrm{PMF}(\alpha) = -k_B\mathrm{T}\ln[P(\alpha)/\sin(\alpha)]$ and a quadratic fit at $[10^\circ, 30^\circ]$ at T = 310 K, where $\sin(\alpha)$ is the probability distribution of a hypothetical non-interacting particle system. A figure on the left presents the PMF profile (the blue solid line) from the upper layer and a quadratic fit (the blue dotted line). A figure on the right shows the same plots from the lower layer.

In order to obtain a quadratic fit of the PMF profile, we use the Curve Fitting Tool of MATLAB. We obtain the following bending moduli at T = 310 K: 17.408 k_BT (the upper layer) and 17.990 k_BT (the lower layer). We take an average of these two values, 17.699 k_BT, as the bending modulus of the DOPC/DOPG mixture at T = 310 K. Figure 12 is the same as Fig. 11, but at T = 288 K. As for the probability distributions of the splay angles, there are no significant changes at T = 288 K. Using the same approach, we get the following bending moduli: 17.428 k_BT (the upper layer) and 16.600 k_BT (the lower layer). Again, we take an average of these two values, 17.014 k_BT, as the bending modulus of the DOPC/DOPG mixture at T = 288 K.

DATA AVAILABILITY

The data that support the findings of this study are available from the corresponding author upon reasonable request.

REFERENCES

[1] G. Guidotti, L.Brambilla, and D. Rossi, Trends Pharmacol. Sci. **38**, 406 (2017).
[2] F. Madani, S. Lindberg, Ü. Langel, S. Futaki, and A. Gräslund, J. Biophys. **2011**, 1.
[3] I. Ruseska and A. Zimmer, Beilstein J. Nanotechnol. **11**, 101 (2020).
[4] J. Pae, P. Säälik, L. Liivamägi, D. Lubenets, P. Arukuusk, Ü. Langel, and M. Pooga, J. Controlled Release **192**, 103 (2014).
[5] Y. Pouny, D. Rapaport, A. Mor, P. Nicolas, and Y. Shai, Biochemistry **31**, 12416 (1992).
[6] K. Matsuzaki, S. Yoneyama, O. Murase, and K. Miyajima, Biochemistry **35**, 8450 (1996).
[7] D. Derossi, S. Calvet, A. Trembleau, A. Brunissen, G. Chassaing, and A. Prochiantz, J. Biol. Chem. **271**, 18188 (1996).
[8] M.-T. Lee, W.-C. Hung, F.-Y. Chen, and H. W. Huang, Biophys. J. **89**, 4006 (2005).
[9] M. M. Fretz, N. A. Penning, S. Al-Taei, S. Futaki, T. Takeuchi, I. Nakase, G. Storm, and A. T. Jones, Biochem. J. **403**, 335 (2007).
[10] R. Wallbrecher, T. Ackels, R. A. Olea, M. J. Klein, L. Caillon, J. Schiller, P. H. Bovée-Geurts, T. H. van Kuppevelt, A. S. Ulrich, M. Spehr, M. J. W. Adjobo-Hermans, and R. Brock, J. Controlled Release **256**, 68 (2017).
[11] K. Melikov, A. Hara, K. Yamoah, E. Zaitseva, E. Zaitsev, and L. V. Chernomordik, Biochem. J. **471**, 221 (2015).
[12] E. Eiríksdóttir, K. Konate, Ü. Langel, G. Divita, and S. Deshayes, Biochim. Biophys. Acta, Biomembr. **1798**, 1119 (2010).
[13] M. Z. Islam, S. Sharmin, M. Moniruzzaman, and M. Yamazaki, Appl. Microbiol. Biotechnol. **102**, 3879 (2018).
[14] H. D. Herce, A. E. Garcia, J. Litt, R. S. Kane, P. Martin, N. Enrique, A. Rebolledo, and V. Milesi, Biophys. J. **97**, 1917 (2009).
[15] H. D. Herce and A. E. Garcia, Proc. Natl. Acad. Sci. U. S. A. **104**, 20805 (2007).
[16] M. A. Crosio, M. A. Via, C. I. Cámara, A. Mangiarotti, M. G. Del Pópolo, and N. Wilke, Biomolecules **9**, 625 (2019).
[17] J. C. Phillips, R. Braun, W. Wang, J. Gumbart, E. Tajkhorshid, E. Villa, C. Chipot, R. D. Skeel, L. Kalé, and K. Schulten, J. Comput. Chem. **26**, 1781 (2005).
[18] B. R. Brooks, C. L. Brooks III, A. D. Mackerell, Jr., L. Nilsson, R. J. Petrella, B. Roux, Y. Won, G. Archontis, C. Bartels, S. Boresch, A. Caflisch, L. Caves, Q. Cui, A. R. Dinner, M. Feig, S. Fischer, J. Gao, M. Hodoscek, W. Im, K. Kuczera, T. Lazaridis, J. Ma, V. Ovchinnikov, E. Paci, R. W. Pastor, C. B. Post, J. Z. Pu, M. Schaefer, B. Tidor, R. M. Venable, H. L. Woodcock, X. Wu, W. Yang, D. M. York, and M. Karplus, J. Comput. Chem. **30**, 1545 (2009).
[19] S. Jo, T. Kim, V. G. Iyer, and W. Im, J. Comput. Chem. **29**, 1859 (2008).
[20] W. Humphrey, A. Dalke, and K. Schulten, J. Mol. Graphics **14**, 33 (1996).
[21] A. Walrant, A. Vogel, I. Correia, O. Lequin, B. E. S. Olausson, B. Desbat, S. Sagan, and I. D. Alves, Biochim. Biophys. Acta, Biomembr. **1818**, 1755 (2012).
[22] B. Roux, Biophys. J. **95**, 4205 (2008).
[23] J. A. Freites, D. J. Tobias, G. von Heijne, and S. H. White, Proc. Natl. Acad. Sci. U. S. A. **102**, 15059 (2005).
[24] S. Dorairaj and T. W. Allen, Proc. Natl. Acad. Sci. U. S. A. **104**, 4943 (2007).
[25] J. L. MacCallum, W. F. D. Bennett, and D. P. Tieleman, J. Gen. Physiol. **129**, 371 (2007).
[26] G. Grasso, S. Muscat, M. Rebella, U. Morbiducci, A. Audenino, A. Danani, and M. A. Deriu, J. Biomech. **73**, 137 (2018).
[27] G. Khelashvili, G. Pabst, and D. Harries, J. Phys. Chem. B **114**, 7524 (2010).
[28] G. Khelashvili, B. Kollmitzer, P. Heftberger, G. Pabst, and D. Harries, J. Chem. Theory Comput. **9**, 3866 (2013).
[29] Z. A. Levine, R. M. Venable, M. C. Watson, M. G. Lerner, J.-E. Shea, R. W. Pastor, and F. L. H. Brown, J. Am. Chem. Soc. **136**, 13582 (2014).
[30] J. Steinkühler, P. D. Tillieux, R. L. Knorr, R. Lipowsky, and R. Dimova, Sci. Rep. **8**, 11838 (2018).
[31] Z.-L. Li, H.-M. Ding, and Y.-Q. Ma, Soft Matter **9**, 1281 (2013).
[32] J.-M. Hu, W.-D. Tian, and Y.-Q. Ma, Macromol. Theory Simul. **24**, 399 (2015).
[33] O. Maniti, H.-R. Piao, and J. Ayala-Sanmartin, Int. J. Biochem. Cell Biol. **50**, 73 (2014).
[34] P. Sens, L. Johannes, and P. Bassereau, Curr. Opin. Cell Biol. **20**, 476 (2008).
[35] B. J. Reynwar, G. Illya, V. A. Harmandaris, M. M. Müller, K. Kremer, and M. Deserno, Nature **447**, 461 (2007).
[36] M. Goulian, R. Bruinsma, and P. Pincus, Europhys. Lett. **22**, 145–150 (1993).
[37] H. Agrawal, L. Liu, and P. Sharma, Soft Matter **12**, 8907 (2016).
[38] N. Schmidt, A. Mishra, G. H. Lai, and G. C. L. Wong, FEBS Lett. **584**, 1806 (2010).
[39] S. Yesylevskyy, S.-J. Marrink, and A. E. Mark, Biophys. J. **97**, 40 (2009).
[40] M. C. Zwier, J. L. Adelman, J. W. Kaus, A. J. Pratt, K. F. Wong, N. B. Rego, E. Suárez, S. Lettieri, D. W. Wang, M. Grabe, D. M. Zuckerman, and L. T. Chong, J. Chem. Theory Comput. **11**, 800 (2015).